Analysis of thermal behavior in 3D printing of continuous fiber reinforced polymer composites

Shixian Li, Joâo Pedro de Magalhaes Correia, Kui Wang, Said Ahzi

Materials Research Proceedings 41 (2024) 2573-2583 https://doi.org/10.21741/9781644903131-283

Analysis of thermal behavior in 3D printing of continuous fiber reinforced polymer composites

LI Shixian[1,a,*], CORREIA J.P.M.[1,b], WANG Kui[2,c] and AHZI Said[1,d]

[1]ICUBE Laboratory – CNRS, University of Strasbourg, Strasbourg 67000, France

[2]Key Laboratory of Traffic Safety on Track of Ministry of Education, School of Traffic & Transportation Engineering, Central South University, Changsha, 410075, China

[a]shixian.li@etu.unistra.fr, [b]jpm.correia@unistra.fr, [c]kui.wang@csu.edu.cn, [d]ahzi@unistra.fr

Keywords: 3D Printing, Continuous Fiber, Thermal Behavior, Interfacial Bonding

Abstract. Fused filament fabrication (FFF) as an additive manufacturing process, is a thermal driven method used to produce continuous fiber reinforced composites for engineering applications. Interlayer delamination is a significant concern for composites manufactured by FFF process. To address the problem of interlayer delamination and enhance the macro-mechanical properties of FFF fiber composites, it is necessary to study the thermal behavior of continuous fiber filled composites during the deposition process. A thermal simulation model with the consideration of continuous fiber was proposed. The numerical simulations reproduce the trends of experimental temperature evolution. When the continuous fiber phase is omitted from the heat transfer model, the predicted reheating temperature at the interface is lower compared to the temperature measured via IR monitoring. This result highlights the critical necessity of developing a numerical model that takes the continuous fiber phase into account in order to accurately predict the reheating temperature at the interface. Such a model is essential for deeper exploration into the adhesion mechanisms between adjacent layers and adjacent filaments.

Introduction

Continuous fiber reinforced polymer composites (CFRPCs) have garnered significant interest from both the academic research community and industrial sectors. This is primarily due to their ability to offer a combination of low weight, high strength, and stiffness that outperforms traditional metals and alloys [1, 2]. The production of composites filled with continuous fibers to depend on molding techniques, resulting in high expenses, limited adaptability, and impracticality for producing small batches. These limitations and disadvantages have hindered the capacity of CFRPCs to be utilized in novel structural applications.

The emergence of additive manufacturing (AM), often known as 3D printing, presents a promising resolution for engineering fiber composites. This technology enables the production of components with intricate geometries, attaining remarkable performance levels, and realizing cost savings [3, 4]. As a result, complex components can be quickly manufactured with reduced expenses and without the requirement for specialized equipment [5]. 3D printing is mainly conducted by stereolithography (SLA), fused filament fabrication (FFF), laminated object manufacturing (LOM), selective laser sintering (SLS), selective laser melting (SLM), etc. One of the most commonly employed AM processes is FFF, which manufactures composites layer-by-layer deposition of extruded molten material [6-8]. Specifically, due to the FFF continuous processing characteristics, adjacent strands come into touch with one another and create a bonding interface that is typically weak and prone to failure [9, 10]. Therefore, an essential issue in printing materials with good mechanical properties is the bonding quality between the solidified strands [11-14].

Bellehumeur et al. [15] proposed that the merging of continuous filament segments occurred through a series of stages including contact, wetting, and neck growth. These phases were induced through the sintering or thermal diffusion of adjacent layers, necessitating temperatures surpassing the material's glass-transition temperature (Tg). Moreover, as presented in [16, 17], the arrangement and evolution of temperature distribution during the FFF process for polymer composites proved to be a pivotal element influencing diverse attributes including geometric precision, surface finish, mechanical strength, and macro and micro-porosity. These characteristics were impacted by the chosen process parameters, encompassing factors like the material being printed, nozzle temperature, printing speed, infill design, deposition order, and layer thickness. Consequently, the thermal history of the printed composite holds importance in determining the ultimate mechanical performance of the end product.

To obtain optimal process conditions, numerous experiments are needed to investigate and optimize the process parameters within given machines and processes by using contact sensors or non-contact sensors [18-20]. Montecon et al. [21] investigated the effect of the interlayer cooling and consequent bonding behavior in printed PLA-based composites by using the thermal imaging method and tensile tests. In [21], it was found that the additional waiting times did not present significant differences in the interfacial bonding properties of printed composites. Fen et al. [22] studied the influence of nozzle temperature and bed temperature on the thermal and mechanical attributes of 3D-printed continuous carbon fiber-reinforced composites. They employed K-type thermocouples (contact sensors) for real-time in-situ thermal assessments. In [22], the nozzle temperature was elevated from 180 to 220 °C, the diameter of the bonding neck expanded from 0.29 to 0.34 mm, leading to a decline in cross-sectional porosity from 5.48 % to 3.22 %.

However, it is rather time-consuming and expensive to produce components with sound geometric configuration and good mechanical properties using FDM by a trial-and-error approach. Hamid Reza et al. [23] employed a 1D heat transfer model to predict temperature variations in a single PLA filament and a vertical PLA wall. In a subsequent study [24], they introduced the finite volume method to describe the overall heat transfer phenomena occurring during the manufacturing sequence. This approach considered three potential mechanisms: conduction between filaments, conduction between filament and support, and free convection with the environment. The predicted results demonstrated a satisfactory agreement when compared to the recorded temperature variations at the interface of adjacent filaments in a printed PLA vertical wall. In [25, 26], researchers also built a 2D or 3D heat transfer modeling to predict temperature evolution of PEKK and ABS, respectively. The recent studies most focus on the thermal prediction of pure polymer matrix materials in FFF process, with insufficient attention given to continuous fiber composites. However, the introduction of continuous fibers in printing brings about alterations in physical parameters during heat transfer and shrinkage, consequently influencing the resin diffusion process on the base and the size of the bonding neck between the printing raster.

In this study, a polypropylene based composite with continuous ramie fiber reinforcement was manufactured by the FFF method. The thermal behavior was investigated by using an in-situ thermal behavior monitoring platform, consisting of an infrared camera, laptop and printed composites. A novel thermal simulation model with the consideration of continuous fiber was proposed. Effect of layer thickness on effective reheating temperature and weld time in continuous ramie fiber-reinforced PP-based composites were investigated.

Experimental Methodology

Materials

In this study, Polypropylene (PP) filaments (grade 9025, Sabic, Saudi Arabia) were selected as the thermoplastic matrix material for continuous ramie fiber-reinforced PP-based composites (CRFRPCs). The reinforcement chosen for CRFRPCs in this study are continuous ramie fiber filaments sourced from Hunan Huasheng Dongting Ramie Textile Co., Ltd, Hunan, China. The

composition of the ramie yarn, assessed through the Van Soest method, revealed the following components: 73.6% cellulose, 13.8% hemicellulose, 3.5% pectin, 1.9% lignin, and 7.2% other constituents [27]. Before the FFF process, the ramie yarns underwent a drying procedure in an oven at 80 °C for a duration of two hours.

Manufacturing

3D-printed composites incorporating continuous ramie fibers were fabricated using an in-situ impregnation desk printer, specifically the Combot-200 from Fibertech in Shanxi, China. The printer utilized a single flat-head nozzle with a diameter of 1.3 mm. The experimental setup of the printing process is illustrated in Fig. 1 (a).

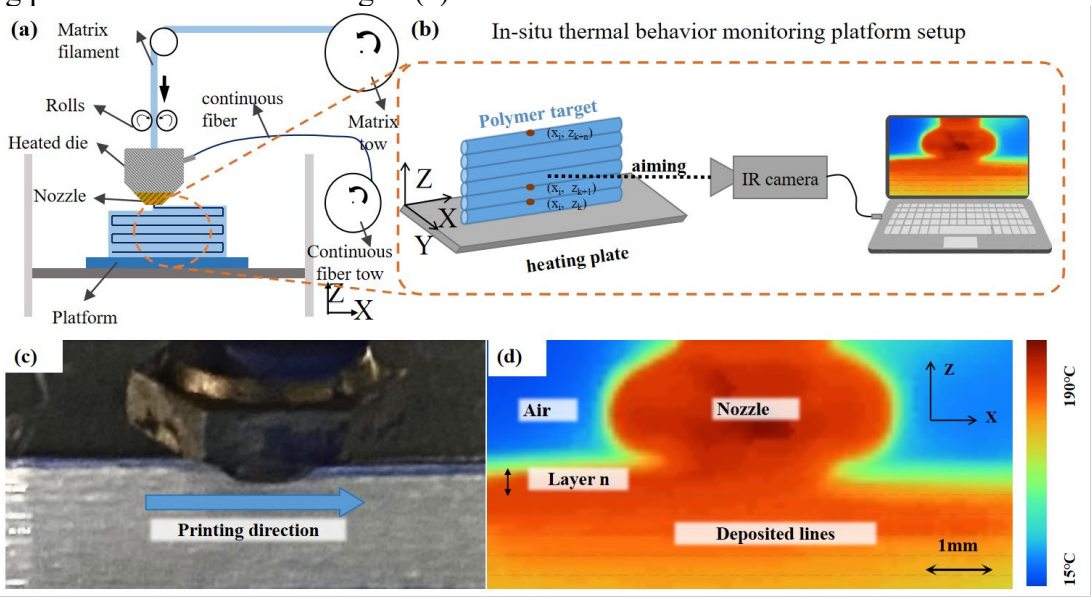

Fig. 1 Schematic representation of the (a) in-situ impregnation process in FFF for continuous fiber filled composites, (b) of the setup for in-situ thermal behavior monitoring platform during FFF. (c) Optical image by camera and (d) thermal image captured by IR camera during FFF process.

In this process, the thermoplastic PP matrix was raised to a temperature exceeding its melting point within the nozzle. Concurrently, the dry continuous ramie fibers underwent pre-heating within the heated die. Subsequently, the impregnated ramie fiber yarns and the molten PP matrix were extruded together from the nozzle and promptly deposited. This facilitated the in-situ impregnation of the ramie yarns with the PP matrix. The deposition was systematically placed onto the printing platform, gradually forming each component layer by layer. Key parameters governing the process, including layer thickness, printing speed, nozzle temperature, and bed temperature, were configured as follows: 0.3 mm, 100 mm/min, 190 °C, and 50 °C, respectively [28, 29].

Differential scanning calorimetry test

Differential Scanning Calorimetry (TG/DSC1, Mettler-Toledo) was employed to determine the crystallization and melting temperatures of the CRFRPCs after the completion of the printing process. The experiment was carried out in a nitrogen atmosphere, with a sample weighing (5.9 ± 0.8) mg. The sample underwent heating from room temperature to 200°C at a consistent rate of 10 °C per minute [30] and cooling back to room temperature naturally. It could be measured that the crystallization temperature (Tc) and melting temperature (Tm) of sample was 121.45 ℃ and 152.05 ℃ in this range of study, as shown in Fig. 2.

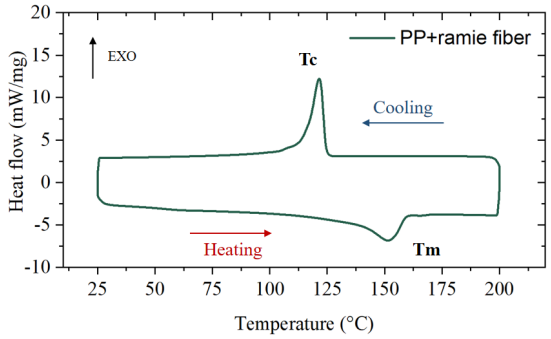

Fig. 2 DSC curves for printed CRFRPCs specimen

Thermography

For this study, an infrared (IR) camera, specifically the Mengchen MCDC-310 from Hunan Ruoxin Co., Ltd in China, was chosen. The IR camera operates within a wavelength range of 7.5-14 μm, has a sampling frequency of 50 Hz, an optical resolution of 384×288 pixels, spatial resolution of 17 μm/pixel, and a working distance ranging from 50 to 90 cm. Fig. 1 (b) depicts the schematic representation of the in-situ thermal behavior monitoring platform.

The geometry of the single wall-shaped composites measured 60×2.2×50 mm, as illustrated in Fig. 1 (b). When the object was oriented along the machine's Cartesian system, the IR camera captured the evolution of temperature over time within the object's frontal x-z plane. This process recorded temporal temperature variations within the object's frontal plane, specifically monitoring temperature fluctuations at a designated position (x_i, z_k). For example, this observation encompassed both primary reheating, resulting from the deposition of the upper neighbor (x_i, z_{k+1}), and secondary reheating, stemming from the deposition of the subsequent neighbor (x_i, z_{k+2}), …, and nth times reheating, induced by the deposition of the nth neighbor (x_i, z_{k+n}).

Theoretical Methodology

Heat transfer modeling for FFF process

This section introduces the modeling of heat transfer model in the filament during the FFF process. And assumptions of isotropic thermal behavior of materials and constant heat exchange coefficient values are used in this model. The fixed domain utilized is illustrated in Fig. 3, representing a vertical wall constructed with a single filament in the thickness. FFF is purely a thermal process that is explained by the heat transfer governing equation [31, 32] given by Eq. (1):

$$\rho C_P \frac{\partial T}{\partial t} = k\nabla^2 T + \dot{q} \tag{1}$$

where T, ρ, C_P, k, $\dot{q}$ are temperature, density, specific heat, thermal conductivity, and the internal heat generated of part due to the heated nozzle. The initial temperature ($T_{initial}$) is imposed by the extruder. Subsequently, the filament undergoes cooling through convection and radiation interactions with the surrounding air at $T_{environment}$ (representing ② and Ω in Fig. 3 (a). Additionally, it experiences cooling through conduction with the previously extruded filament (indicated as boundary ③ in Fig. 3 (a)). The support plate is kept at T_{plate} and the filaments were reheating by plate with conductive transfer (corresponding to ① in Fig. 3 (a)). It's worth noting that thermal contact resistances between filaments play a role in influencing the conductive transfer, particularly along boundaries ① and ③ as depicted in Fig. 3 (a). The initial and boundary condition are described as follows:

$$T(t=0) = T_{initial} = T_{extrusion} \tag{2}$$

$$q_{convective} = h(T - T_{environment}) \tag{3}$$

$$q_{radiative} = \varepsilon\sigma(T^4 - T_{environment}^4) \tag{4}$$

where $q_{convective}$, $q_{radiative}$, h, $T_{environment}$, ε, σ represent heat flux due to convection, heat flux due to radiation, heat convection coefficient, environment temperature of the surrounding air, material's emissivity, and the Stefan-Boltzmann constant, respectively.

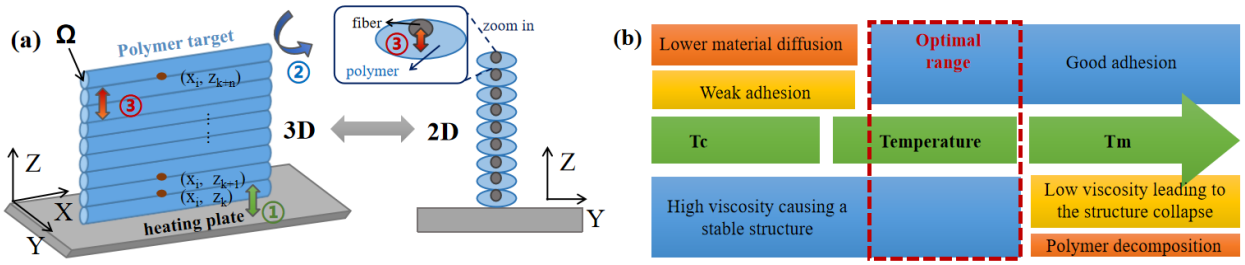

Fig. 3 (a) Geometry and boundary conditions applied in the heat transfer model. (b) Polymer printability rules for FFF process

As depicted in Fig. 3 (b), maintaining an adequately elevated temperature is crucial to facilitate effective healing at the filament interfaces. However, it is equally essential to ensure that this temperature remains within an optimal range to prevent structural collapse, which can result from excessively low viscosity or the potential risks of thermal degradation or chemical aging of the extruded polymer. Additionally, the adhesive bonding between adjacent layers is significantly influenced by the thermal behavior of the printed composites, given the layer-by-layer deposition method [11]. Therefore, a detailed investigation into how thermal properties impact interfacial bonding performance was necessary. Specifically, focusing on the effective temperature range between the Tc at 121.45 ℃ and the Tm at 152.05 ℃ of semi-crystalline polymers emerged as a crucial consideration during the FFF process.

Finite Element Simulation Model

To analysis the FFF process including heat transfer, a transient heat transfer model was solved using the commercial finite element (FE) software Abaqus in this study as shown in Fig. 3 (a) and Fig. 4. The geometry of the polymer filaments' model is a stack of rectangles with rounded corners, and of the continuous fiber yarn' model is an ellipse, mirroring the structure of the printed object during the FFF process. The height and width of polymer filament are 0.3 mm and 1.0 mm, respectively. The fiber's height is defined as 0.1 mm, and the width is 0.26 mm. The cross-sectional size, and position of the continuous fiber yarns in each layer are based on [33]. To facilitate comparison with pyrometer measurements, the simulated temperature was evaluated at a specific point situated on interface between adjacent layers, as illustrated in Fig. 3 (a).

The FE simulation incorporates the deposition of each filament, resulting in a dynamic alteration of geometry and boundary conditions in the numerical model for every new filament. Convective heat transfer and radiative heat transfer are modeled on all interfaces interacting with the air. A consistent temperature is enforced at the bottom boundary of the heating plate. Thermal contact resistance is applied with a constant value at the plate-filament interface and another constant value at the filament-filament interface. The temperature of newly deposited filaments is set to $T_{extrusion}$, as depicted in Fig. 4 (b). The convective coefficients h and material's emissivity coefficient ε are 150 W/(m^2·°C) and 0.96, respectively, in the current range of study [34]. The interaction between fiber yarn and polymer matrix, as well as the interaction between adjacent polymer matrix filaments are defined as low contact (100 W/(m^2·°C)) and perfect contact (10^6 W/(m^2·°C)) based on [33, 34].

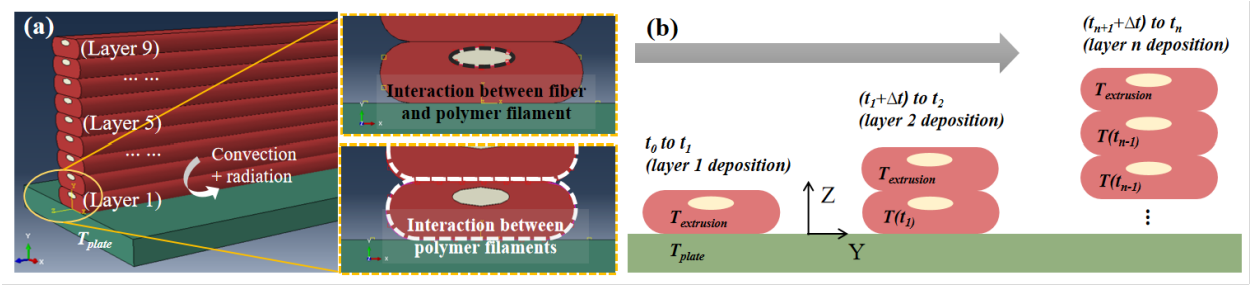

Fig. 4 Model representation, (a) interaction definition between different parts, and (b) with boundary conditions for each new layer deposition.

The thermal properties of PP and ramie fiber were taken from literature [35-39], as shown in table 1. And the process parameters representatives of experimental conditions are reported in the table 2. The component was configured with a mesh comprising 8-nodes linear heat transfer brick elements, specifically DC3D8, and the mesh was incorporated refinement at the corners of the rectangles.

Table 1. Thermal properties used in simulations [35-39].

Properties	**PP**	**Ramie fiber**	**Heating plate**
Density(kg/m^3)	900	1450	2210
Specific heat Cp (J.kg^{-1}K^{-1})	1580	1422	730
Thermal conductivity k (W.m^{-1}K^{-1})	0.27	1.46	1.40

Table 2. Process parameters used for simulations.

Parameters	**PP**	**Ramie fiber**
Extrusion temperature (°C)	190	190
Heating plate temperature (°C)	50	50
Environment temperature (°C)	25	25
Time between 2 filaments deposition (s)	40	40
Layer thickness h (mm)	0.30	0.10
Layer width w (mm)	1.00	0.26

Results and discussion

Simulation results

The temperature predicted at different times is shown in Fig. 5. The simulation outcomes reveal temperature heterogeneity within the filament. Unlike numerous heat transfer models in existing literature that assume a small Biot number, such an assumption is not validated in our case. The interface temperature significantly differs from that observed on the surface through camera monitoring. This reinforces the necessity for a numerical model to accurately estimate the interface temperature.

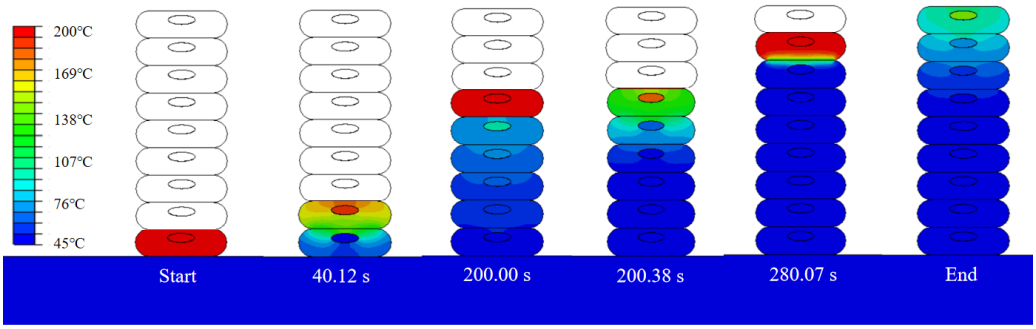

Fig. 5 ABAQUS numerical predictions of temperature (°C) for CRFRPCs during the FFF process.

Validation by experimental results

To validate the thermal results derived from the Abaqus FE model, the evolution of temperature data is compared with that obtained from an IR camera, as detailed in section 2.4. Fig. 6 shows the comparison between simulated and experimental temperature evolutions of layer 1 in CRFRPCs. In Fig. 6, for post-processing analysis, the temperature measurement signals are synchronized at t=0 with reference to the moment of the first temperature peak, considering the highest measured value as the reference at t=0. The curve illustrated in Fig. 6 exhibits a distinct decline after each peak followed by an ascent leading to the subsequent peak. This phenomenon is likely attributed to the reheating effect. Specifically, during the printing process, when a new filament is deposited, the preceding one undergoes a significant cooling phase before being reheated. In literatures [40], the effective reheating peaks, especially for the first reheating processes, were more important for strong interfacial bonding than those of the rest of the reheating peaks. When the temperature of deposited filaments decreases below Tc, the growth of the bonding neck between filaments ceases. Therefore, it is necessary to focus on the first reheating peak whether is within the effective reheating temperature range, to better study the degree of bonding between adjacent layers. Specifically, the predicted value of the first reheating temperature is 127.3 °C, compared with the measured value of 127.9 °C, the difference between each other is small. The numerical simulations reproduce the experimental trends in temperature variation. However, the Abaqus FE model exhibits a faster and more consistent cooling process, potentially attributed to factors such as ideal operating conditions (environment temperature and bed temperature), and limitations in accurately reflecting the material's crystallization behavior within the model.

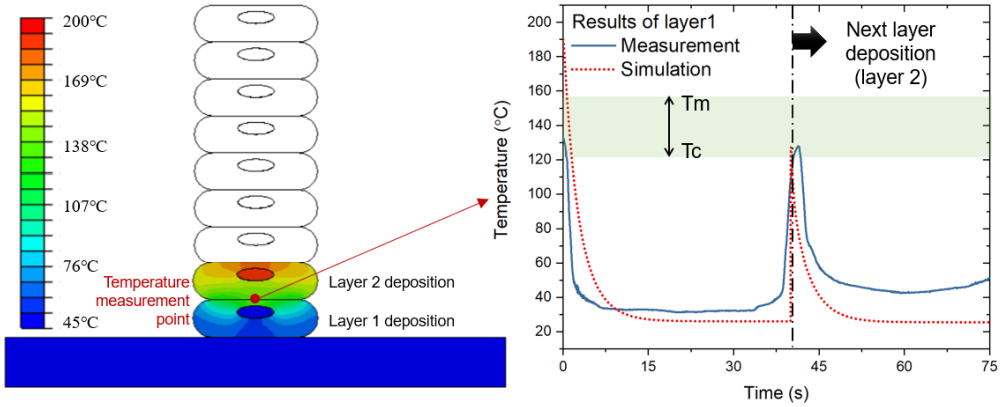

Fig. 6 Comparison of experimental and simulated temperature evolutions of layer1.

Fig. 7 shows the numerical predictions with and without considering the presence of continuous fiber. For the model without considering the continuous fiber, the predicted first reheating temperature value (102.2°C) is much lower than that of the model with considering the presence of continuous fiber phase and lower compared to the value measured by experiment. Thus, we conclude that the presence of fiber may increase the degree of reheating.

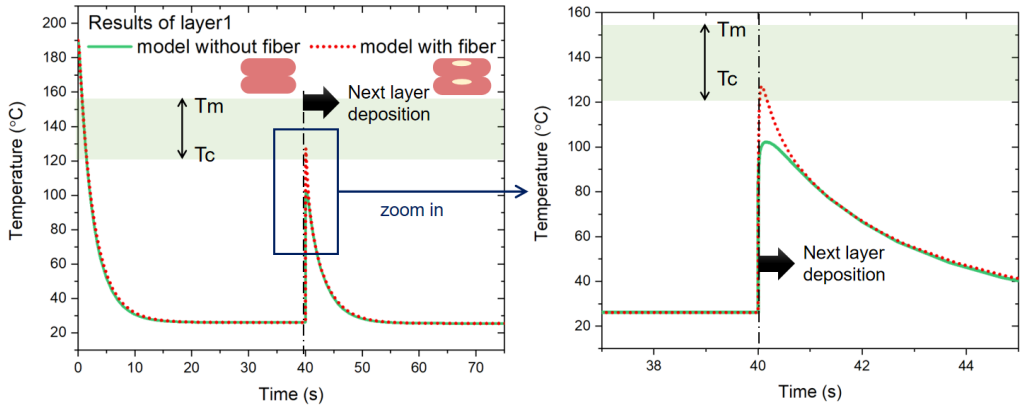

Fig. 7 Simulated results without/with considering the presence of fiber in heat transfer model.

Conclusion

Fused Filament Fabrication (FFF), an additive manufacturing process driven by thermal mechanisms, is employed for the production of continuous fiber-reinforced composites in various engineering applications. Face to the challenge posed by interlayer delamination of FFF composites, improved adhesive bonding is required to improve the macro-mechanical properties of material extrusion 3D printed fiber composites. It is necessary to study the thermal behavior of continuous fiber filled composites in the manufacturing process. This study introduces a novel thermal simulation FE model, incorporating continuous fiber considerations, for heat transfer modeling.

The numerical simulations reproduce the experimental trends in temperature variation. The effective reheating temperature of model is 127.3 °C, compared with the measured value of 127.9 °C. When continuous fiber phase is not considered into the heat transfer model, the reheating temperature at the interface is lower than that of the temperature observed via IR monitoring. This finding underscores the imperative need for a numerical model to precisely estimate the interface's reheating temperature by considering with fiber phase, to further investigate the adhesion between adjacent layers and filaments.

References

[1] Naser M, Hawileh R, Abdalla J. Fiber-reinforced polymer composites in strengthening reinforced concrete structures: A critical review. Engineering Structures. 2019;198:109542. https://doi.org/10.1016/j.engstruct.2019.109542

[2] Bakis CE, Bank LC, Brown V, Cosenza E, Davalos J, Lesko J, et al. Fiber-reinforced polymer composites for construction—State-of-the-art review. Journal of composites for construction. 2002;6(2):73-87. https://doi.org/10.1061/(ASCE)1090-0268(2002)6:2(73)

[3] Chacón J, Caminero M, Núñez P, García-Plaza E, García-Moreno I, Reverte J. Additive manufacturing of continuous fibre reinforced thermoplastic composites using fused deposition modelling: Effect of process parameters on mechanical properties. Composites science and technology. 2019;181:107688. https://doi.org/10.1016/j.compscitech.2019.107688

[4] Ngo TD, Kashani A, Imbalzano G, Nguyen KT, Hui D. Additive manufacturing (3D printing): A review of materials, methods, applications and challenges. Composites Part B: Engineering. 2018;143:172-96. https://doi.org/10.1016/j.compositesb.2018.02.012

[5] Cheng P, Peng Y, Li S, Rao Y, Le Duigou A, Wang K, et al. 3D printed continuous fiber reinforced composite lightweight structures: A review and outlook. Composites Part B: Engineering. 2023;250:110450. https://doi.org/10.1016/j.compositesb.2022.110450

[6] Rinaldi M, Ghidini T, Cecchini F, Brandao A, Nanni F. Additive layer manufacturing of poly (ether ether ketone) via FDM. Composites Part B: Engineering. 2018;145:162-72. https://doi.org/10.1016/j.compositesb.2018.03.029

[7] Cheng P, Peng Y, Wang K, Le Duigou A, Yao S, Chen C. Quasi-static penetration property of 3D printed woven-like ramie fiber reinforced biocomposites. Composite Structures. 2023;303:116313. https://doi.org/10.1016/j.compstruct.2022.116313

[8] Zhao H, Liu X, Zhao W, Wang G, Liu B. An Overview of Research on FDM 3D Printing Process of Continuous Fiber Reinforced Composites. Journal of Physics: Conference Series: IOP Publishing; 2019. p. 052037. https://doi.org/10.1088/1742-6596/1213/5/052037

[9] Seppala JE, Migler KD. Infrared thermography of welding zones produced by polymer extrusion additive manufacturing. Additive manufacturing. 2016;12:71-6. https://doi.org/10.1016/j.addma.2016.06.007

[10] Zhou M, Zhou X, Si L, Chen P, Li M, Zhang Y, et al. Modeling of bonding strength for Fused Filament Fabrication considering bonding interface evolution and molecular diffusion. Journal of Manufacturing Processes. 2021;68:1485-94. https://doi.org/10.1016/j.jmapro.2021.06.064

[11] Seppala JE, Han SH, Hillgartner KE, Davis CS, Migler KB. Weld formation during material extrusion additive manufacturing. Soft matter. 2017;13(38):6761-9. https://doi.org/10.1039/C7SM00950J

[12] Sun Q, Rizvi G, Bellehumeur C, Gu P. Effect of processing conditions on the bonding quality of FDM polymer filaments. Rapid prototyping journal. 2008. https://doi.org/10.1108/13552540810862028

[13] Costa S, Duarte F, Covas J. Estimation of filament temperature and adhesion development in fused deposition techniques. Journal of Materials Processing Technology. 2017;245:167-79. https://doi.org/10.1016/j.jmatprotec.2017.02.026

[14] Touchard F, Chocinski-Arnault L, Fournier T, Magro C, Lafitte A, Caradec A. Interfacial adhesion quality in 3D printed continuous CF/PA6 composites at filament/matrix and interlaminar scales. Composites Part B: Engineering. 2021;218:108891. https://doi.org/10.1016/j.compositesb.2021.108891

[15] Bellehumeur C, Li L, Sun Q, Gu P. Modeling of bond formation between polymer filaments in the fused deposition modeling process. Journal of manufacturing processes. 2004;6(2):170-8. https://doi.org/10.1016/S1526-6125(04)70071-7

[16] Vanaei H, Deligant M, Shirinbayan M, Raissi K, Fitoussi J, Khelladi S, et al. A comparative in-process monitoring of temperature profile in fused filament fabrication. Polymer Engineering & Science. 2021;61(1):68-76. https://doi.org/10.1002/pen.25555

[17] Roy M, Yavari R, Zhou C, Wodo O, Rao P. Prediction and experimental validation of part thermal history in the fused filament fabrication additive manufacturing process. Journal of Manufacturing Science and Engineering. 2019;141(12). https://doi.org/10.1115/1.4045056

[18] Wang K, Li S, Rao Y, Wu Y, Peng Y, Yao S, et al. Flexure Behaviors of ABS-Based Composites Containing Carbon and Kevlar Fibers by Material Extrusion 3D Printing. Polymers. 2019;11(11):1878. https://doi.org/10.3390/polym11111878

[19] Heidari-Rarani M, Rafiee-Afarani M, Zahedi A. Mechanical characterization of FDM 3D printing of continuous carbon fiber reinforced PLA composites. Composites Part B: Engineering. 2019;175:107147. https://doi.org/10.1016/j.compositesb.2019.107147

[20] Cui H, Thomson D, Pellegrino A, Wiegand J, Petrinic N. Effect of strain rate and fibre rotation on the in-plane shear response of±45° laminates in tension and compression tests. Composites Science and Technology. 2016;135:106-15. https://doi.org/10.1016/j.compscitech.2016.09.016

[21] Mantecón R, Rufo-Martín C, Castellanos R, Diaz-Alvarez J. Experimental assessment of thermal gradients and layout effects on the mechanical performance of components manufactured by fused deposition modeling. Rapid Prototyping Journal. 2022. https://doi.org/10.1108/RPJ-12-2021-0329

[22] Fan C, Shan Z, Zou G, Zhan L, Yan D. Interfacial bonding mechanism and mechanical performance of continuous fiber reinforced composites in additive manufacturing. Chinese Journal of Mechanical Engineering. 2021;34(1):1-11. https://doi.org/10.1186/s10033-021-00538-7

[23] Vanaei HR, Shirinbayan M, Costa SF, Duarte FM, Covas JA, Deligant M, et al. Experimental study of PLA thermal behavior during fused filament fabrication. Journal of Applied Polymer Science. 2021;138(4):49747. https://doi.org/10.1002/app.49747

[24] Vanaei HR, Khelladi S, Deligant M, Shirinbayan M, Tcharkhtchi A. Numerical Prediction for Temperature Profile of Parts Manufactured using Fused Filament Fabrication. Journal of Manufacturing Processes. 2022;76:548-58. https://doi.org/10.1016/j.jmapro.2022.02.042

[25] Lepoivre A, Boyard N, Levy A, Sobotka V. Methodology to assess interlayer quality in the material extrusion process: A temperature and adhesion prediction on a high performance polymer. Additive Manufacturing. 2022;60:103167. https://doi.org/10.1016/j.addma.2022.103167

[26] Mahmoud Y, Lyu J, Akhavan J, Xu K, Manoochehri S. Thermal history based prediction of interlayer bond strength in parts manufactured by material extrusion additive manufacturing. The International Journal of Advanced Manufacturing Technology. 2023:1-17. https://doi.org/10.21203/rs.3.rs-2413996/v1

[27] Van Soest Pv, Robertson JB, Lewis BA. Methods for dietary fiber, neutral detergent fiber, and nonstarch polysaccharides in relation to animal nutrition. Journal of dairy science. 1991;74(10):3583-97. https://doi.org/10.3168/jds.S0022-0302(91)78551-2

[28] Lei L, Yao Z, Zhou J, Wei B, Fan H. 3D printing of carbon black/polypropylene composites with excellent microwave absorption performance. Composites Science and Technology. 2020;200:108479. https://doi.org/10.1016/j.compscitech.2020.108479

[29] Morales MA, Atencio Martinez CL, Maranon A, Hernandez C, Michaud V, Porras A. Development and characterization of rice husk and recycled polypropylene composite filaments for 3D printing. Polymers. 2021;13(7):1067. https://doi.org/10.3390/polym13071067

[30] Vanaei H, Shirinbayan M, Deligant M, Raissi K, Fitoussi J, Khelladi S, et al. Influence of process parameters on thermal and mechanical properties of polylactic acid fabricated by fused filament fabrication. Polymer Engineering & Science. 2020;60(8):1822-31. https://doi.org/10.1002/pen.25419

[31] Nath P, Olson JD, Mahadevan S, Lee Y-TT. Optimization of fused filament fabrication process parameters under uncertainty to maximize part geometry accuracy. Additive manufacturing. 2020;35:101331. https://doi.org/10.1016/j.addma.2020.101331

[32] Xu D, Zhang Y, Pigeonneau F. Thermal analysis of the fused filament fabrication printing process: Experimental and numerical investigations. International Journal of Material Forming. 2021;14:763-76. https://doi.org/10.1007/s12289-020-01591-8

[33] Cheng P, Wang K, Chen X, Wang J, Peng Y, Ahzi S, et al. Interfacial and mechanical properties of continuous ramie fiber reinforced biocomposites fabricated by in-situ impregnated 3D printing. Industrial Crops and Products. 2021;170:113760. https://doi.org/10.1016/j.indcrop.2021.113760

[34] Costa S, Duarte F, Covas J. Thermal conditions affecting heat transfer in FDM/FFE: a contribution towards the numerical modelling of the process: This paper investigates convection, conduction and radiation phenomena in the filament deposition process. Virtual and Physical Prototyping. 2015;10(1):35-46. https://doi.org/10.1080/17452759.2014.984042

[35] Lepoivre A, Boyard N, Levy A, Sobotka V. Heat transfer and adhesion study for the FFF additive manufacturing process. Procedia manufacturing. 2020;47:948-55. https://doi.org/10.1016/j.promfg.2020.04.291

[36] Patti A, Acierno D. Thermal conductivity of polypropylene-based materials. Polypropylene—Polymerization And Characterization Of Mechanical And Thermal Properties. 2020. https://doi.org/10.5772/intechopen.84477

[37] Weidenfeller B, Höfer M, Schilling FR. Thermal conductivity, thermal diffusivity, and specific heat capacity of particle filled polypropylene. Composites Part A: applied science and manufacturing. 2004;35(4):423-9. https://doi.org/10.1016/j.compositesa.2003.11.005

[38] Lodha P, Netravali AN. Characterization of interfacial and mechanical properties of “green” composites with soy protein isolate and ramie fiber. Journal of materials science. 2002;37:3657-65. https://doi.org/10.1023/A:1016557124372

[39] Maddah HA. Polypropylene as a promising plastic: A review. Am J Polym Sci. 2016;6(1):1-11.

[40] Basgul C, Thieringer FM, Kurtz SM. Heat transfer-based non-isothermal healing model for the interfacial bonding strength of fused filament fabricated polyetheretherketone. Additive Manufacturing. 2021;46:102097. https://doi.org/10.1016/j.addma.2021.102097